Petroleum and Coal

Article **Open Access**

Design of Novel Synthetic Iron Oxide Nano-Catalyst over Homemade Nano-Alumina for an Environmentally Friendly Fuel: Experiments and Modelling

Aysar T. Jarullah [1], Ban A. Al-Tabbakh[2], Mustafa A. Ahmed [1], Shymaa A. Hameed [1], Iqbal M. Mujtaba[3]*

[1] *Chemical Engineering Department, College of Engineering, Tikrit University, Iraq*
[2] *Petroleum Research & Development Center, The Iraqi Ministry of Oil / Baghdad, Iraq*
[3] *Chemical Engineering Department, Faculty of Engineering & Informatics, University of Bradford, Bradford BD7 1DP, UK*

Received January 12, 2022; Accepted June 14, 2022

Abstract

Achieving an environmentally friendly fuel with respect to minimum sulfur compounds has recently became a significant issue for petroleum refining industries. This paper focuses on investigating oxidative desulfurization (ODS) process for removal of sulfur compounds found in light gas oil (LGO) in a batch reactor (at different reaction temperatures and batch time) using a novel nano-catalyst based on 4% iron oxide (Fe_2O_3) as an active component. Precipitation and Impregnation methods are used to prepare the nano-gamma alumina (γ-alumina) and to generate the new synthetic homemade nanocatalyst. A mathematical model is formulated for the ODS process to estimate the optimal kinetic parameters within gPROMS package. An excellent consistency with the experimental data of all runs with error less than 5% have obtained. The optimization results display that the new nanocatalyst prepared here is effective in removing more than 97% of the sulfur compounds from LGO resulting in a cleaner fuel.

Keywords: *Nano-catalyst; Parameters estimation; Iron oxide; Gamma alumina; Mathematical model.*

1. Introduction

In recent years, growing global energy demand, strict environmental legislations on transportation fuels and depleting oil reserves have together formed a triangle of constraints posing great challenges to refiners. Growing emissions in the form of SO_X will increase with increasing energy demand due to combustion of fuels in transportation or in oil refineries. These emissions are harmful because of the emitted sulfur dioxide (SO_X) can react with water in the atmosphere forming acidic rains that harmful to soil, buildings, forests and ecosystems [1-3]. Also, sulfur emissions lead to aggravate heart illness, respiratory illnesses, trigger asthma and contribute to the formation of atmospheric particulates [4].

Sulfur compounds in fuel oil can be classified into four main groups mercaptans, thiophenes (TH), benzothiophenes (BT), and dibenzothiophenes (DBT) [5]. As a result, environmental regulations on the sulfur level are legislated in transportation fuels to reduce the sulfur content in diesel to less than 10 ppm since 2005 in Europe, less than 15 ppm since 2006 in the US, and less than 50 ppm since 2008 in Beijing and Shanghai in China and recently less than 10 ppm [6]. Therefore, desulfurization of fuels is very essential process in petroleum industry, and there is a need to find new methods that are more efficient, cost effective meeting the expectations of environmental regulations and refining requirements [7]. Many methods have been applied to remove sulfur compounds from fuel oil, such as hydrodesulfurization (HDS), extractive distillation, selective adsorption, biodesulfurization, and oxidative desulfurization (ODS) [8]. Hydrodesulfurization (HDS) is a common method for sulfur removal, which is used in petroleum refineries, but this process has drawbacks such as higher investment costs, high

operating conditions and low efficiency on DBT [9-12]. Therefore, researchers focus on the non-conventional low cost and low severity processes. So, ODS process is regarded as an alternate technique and considered to be a good choice among them. ODS is considered as a promising desulfurization technology because it can be operated at low temperature and low pressure and does not require the use of hydrogen.

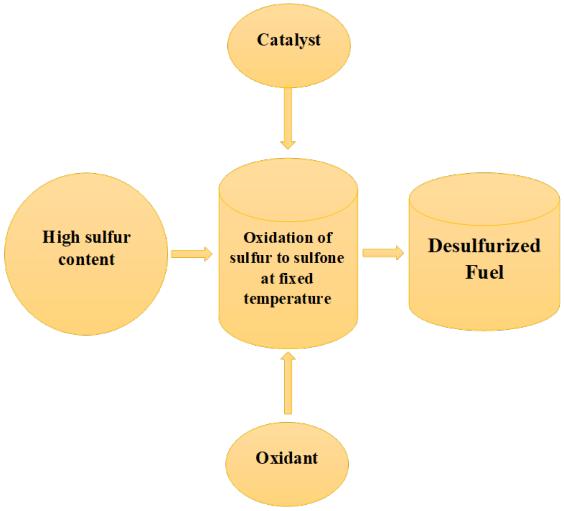

Figure 1. Schematic representation of sulfur removal in the ODS process

Also, ODS process can easily remove the refractory sulfur compounds owing to their high electron density [13-16]. ODS process can enhance the efficiency of sulfur removal without destroying and poisoning catalyst [17]. As shown in Figure 1, the sulfur compounds in fuel oil are oxidized to their respective sulfones or sulfoxides by oxidizing agents. These compounds formed can be easily removed from fuel oil by extraction or adsorption due to their high polarity [11, 18].

The preparation of the catalyst and the choice of oxidant are also considered the main effective factors on the ODS process [19]. In the former works, several types of oxidants have been studied, such as O_2, H_2O_2 and organic peroxides [20-22]. The catalyst plays a very important key role in the ODS process owing to its responsibility for activating oxidants [23]. The catalytic system can be classified into supported and non-supported catalyst.

Supported catalyst consists of support and active metal such as Mn/Al_2O_3 [24], Co-Mo/Al_2O_3 and Ni-Mo/Al_2O_3 [25]. Nano-catalyst can be used in this process where nano-structured materials having much higher activities than that of the corresponding bulk materials [26]. Catalytic activity increases with decreasing the size of the particles [27]. By reducing the domain size of catalyst particle as far as possible, the number of active sites can be maximized [28]. Alumina is widely employed as a catalyst or catalyst support in several chemical processes, such as ammonia synthesis, synthesis gas and hydrogen production, oils hydrogenation, petroleum refining, automotive emissions control, and others [29-30]. Comparing micron-sized alumina particles, nano alumina have many advantages such as high hardness, good wear resistance and outstanding mechanical properties at high-temperature [31-33]. A smaller particle size provides a much larger surface area for molecular collisions and hence increases the rate of reaction, making it a better catalyst and reactant [33]. Iron oxide is used in the oxidative desulfurization process as an active metal in catalyst due to it is inexpensive as compared to other metal oxides, and it has excellent physicochemical properties, such as porosity, high surface and electropositivity [34].

The novelty of this study is to prepare a new homemade nano-catalyst for deep oxidative desulfurization process, which contain Fe_2O_3 as active metal and γ-alumina as support. The loading of Fe_2O_3 on γ-alumina has not been reported in the public domain for ODS process. Also, γ-alumina nanoparticles used as a support of the catalyst is prepared by precipitation method from simple available raw material in addition to the precipitation method that has not been used to prepare γ-alumina as catalyst support for ODS process. As well as, oxidative desulfurization process is carried out by using real light gas oil (LGO) fraction as feedstock in a batch reactor utilizing the air as an oxidant.

The study aims to develop new homemade nano-catalyst for deep oxidative desulfurization process of light gas oil with low cost and less environmental effect via laboratory experiments. The objectives of this study can be summarized as follows:

- Preparation of homemade γ-alumina nanoparticles as support for catalyst.
- Preparation of new nano-catalyst, which is 4% Fe_2O_3 / γ-alumina nanoparticles.

- Investigating the activity of the prepared catalyst via oxidative desulfurization reactions using light gas oil (LGO) fraction as feedstock at different operating conditions in a batch reactor utilizing the air as an oxidant.
- Studying the impact of the main operating variables (temperature and batch time) on the efficiency of desulfurization of the light gas oil.
- Determining the optimal kinetic parameters of the relevant reactions that can be used with high confidence to reactor design via optimization technique (two ways are employed for this purpose (linear and non-linear)).
- Achieving an environmentally friendly fuel by applying the optimization process to get the minimum sulfur content based on the validated model of the prepared nano-catalyst over homemade nano- γ-alumina.

2. Experimental work

2.1. Catalyst preparation

2.1.1. Material

The chemical compounds that used for support and catalyst preparation are explained in Table 1.

Table 1. List of materials and chemicals utilized for support and catalyst preparation

Chemicals	Formula	Molecular weight, g/gmol	Purity %	Supplier
Ferric nitrate hydrate	$Fe(NO_3)_3.9H_2O$	404	98	Himedia
Aluminum nitrate	$(Al(NO_3)_3.9H_2O)$	375.13	97	GCC
Ammonium hydroxide	(NH_4OH)	17.03	28%	GCC
Ethanol	C_2H_5OH	46.07	98	Hayaman

2.1.2. γ-Alumina preparation

In previous studies, the commercial γ-alumina has used as a catalyst support in ODS process [25-26]. In this study, the preparation process of γ-alumina is carried out by precipitation method that has the advantages of high purity, low cost, simple equipment manufacturing, large amount of production and short process beside available raw materials used in this method. So, γ-alumina is prepared here by the such method based on simple available raw material and simple equipment manufacturing.

A weight of (80 g) of $Al(NO_3)_3.9H_2O$ is dissolved in 100 mL of deionized water. Under constant magnetic stirring and in the presence of an ice bath, drops of ammonium hydroxide are added until the solution mixture is turned to foaming solution. The pH of the solution mixture is initially recorded at 2, then gradually increased and raised sharply from 2 to 7.5 during producing γ-alumina. Then, (50 mL of water + 50 mL of ethanol) is mixed and added to the foaming solution to remove any insoluble impurity. The filtered foaming solution is dried by using the furnace at temperature of 120°C for 12 hours. Such behavior causes the foaming solution to transfer to the solid state until the shrinkage in volume and changing in color of the foaming solution from grey to white is noticed. The dried sample is then crushed by hand in mortar to dispose the agglomeration of particles. After that, the samples is calcinated at a temperature of 650°C for 6 hours by using a furnace to obtain the nano γ-alumina and water as illustrated in equations 1 to 4 [35-36]:

$$Al(NO_3)_{3\,(S)} + H_2O \xrightarrow{3NH_4OH} Al(OH)_{3\,(S)} + 3\,NH_4NO_3 + H_2O \quad (1)$$

$$2Al(OH)_{3\,(S)} \xrightarrow{110^oC} Al(OH)_{3\,(S)} + 3\,NH_4NO_3 + H_2O \quad (2)$$

$$2AlO.OH_{\,(S)} \xrightarrow{650^oC} \gamma\text{-}Al_2O_{3\,(S)} + H_2O \quad (3)$$

The process of calcination is carried out at steps where the temperature is increased with rate 6°C/min to 250°C for 1 h then to 450°C for 1 h and finally to 650°C for 4 h. The powder is cooled down until room temperature by switching off the furnace. The next step is crashing the powder, where the utilization active γ-alumina is crashed using a mortar and hammer to obtain final result of the nano activated γ-alumina. The prepared γ-alumina steps are shown in Figure.2.

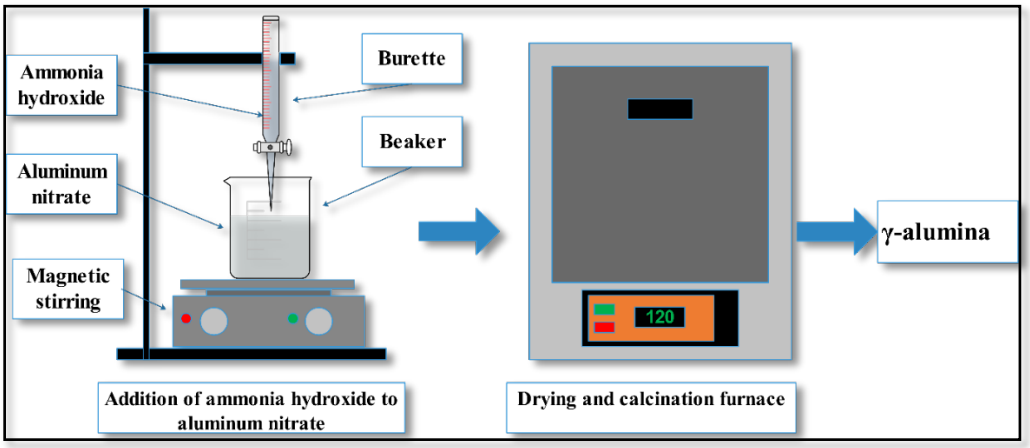

Figure 2. γ-Alumina preparation steps

2.1.3. Preparation of Fe_2O_3/ γ-alumina catalyst

Homemade nano-catalyst (4% Fe_2O_3/γ-alumina) that has not been reported in the public domain in ODS process is prepared here by impregnation method. 0.95 gm of ferric nitrate hydrate is dissolved in 23 mL of deionized water then the solution is stirred by using magnetic stirrer for one hour at room temperature to get the saturated solution. 7.125 gm of the prepared γ-alumina nanoparticles are weighed in a beaker and the solution of ferric nitrate is added to the prepared γ-alumina in the beaker and stirring via magnetic stirrer for one hour at room temperature until the solution is completely impregnated. The impregnated γ-alumina is dried and calcinated in the furnace with four step processes. The solution is charged into beaker and placed in the furnace where temperature is raised to 120°C overnight. After that, the temperature is increased to 400°C for 2 h and finally to 550°C for 3 h to be gradually reduced. The purpose of calcination step is to convert metal salts loaded on γ-alumina to their corresponding metal oxides and deposition of the active metal oxide on the catalyst support. Also, the catalyst has acquired the physical and chemical properties. The prepared catalyst steps are shown in Figure.3.

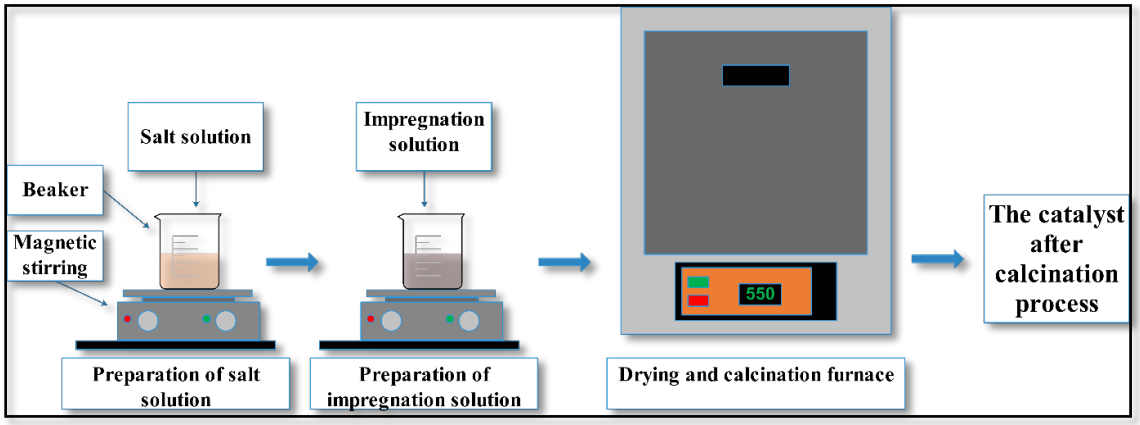

Figure 3. The catalyst preparation steps

2.2. Oxidative desulfurization reactions

2.2.1. Oil feedstock

Light gas oil (total sulfur content = 0.7510 wt %) obtained from KAR refinery/North of Iraq (Erbil) is utilized as liquid feedstock for ODS reaction. The physical properties of the light gas oil are illustrated in Table 2 and tested by the central laboratory of petroleum/ Erbil.

Table 2. Properties of light gas oil feedstock

Physical property	Values	Physical property	Values
Specific gravity at 15.5°C	0.8207	Pour point (°C)	<-20
API gravity	39.23	Distillation	(oC)
Total sulfur content (wt %)	0.7510	Initial boiling point (°C)	195
Kinematic viscosity at 313 K	3.21	10%	212
Flash point, (°C)	73	50%	246
Cetane index	54	90%	300
Cetane number	54	Final boiling point (°C)	328

2.2.2. Batch reactor

The oxidation reaction of sulfur compound is conducted in a batch reactor. Three necks round bottom flask of 500 mL is used for the reaction.

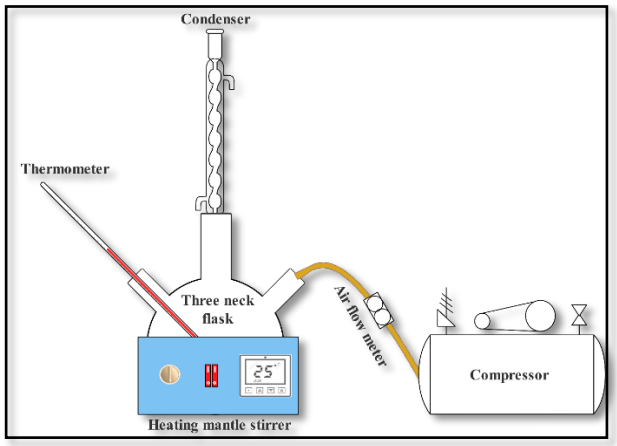

Figure 4. Process diagram of batch reactor system

The middle neck is connected to a vertical condenser to condense the vapor of oil feedstock in order to permit air to leave only. The second neck used as air inlet which connected to compressor and the air will reach to the bottom of the flask by glass tube while the third neck is used to measure the temperature in the flask by inserting a thermometer to the solution inside the flask and to withdraw the sample reaction when the time is approached. The heating and mixing of the batch reactor is carried out via heating mantle stirrer. The process diagram and experimental device of ODS is shown in Figure 4.

2.3. Experimental testing

2.3.1. Operating conditions

In this work, the experimental work includes several runs with respect to ODS process based on the following operating conditions:

- Reaction temperature: 90°C, 110°C, 130°C, 150°C.
- Batch time: 40min, 60min, 80min, 100min.
- The air flow rate is 120 L/h and the pressure is 1atm.

2.3.2. Oxidation of sulfur compounds

The oil feedstock is light gas oil containing sulfur compound. The prepared catalyst and the device are installed to run all the experiments and the following steps are performed in each run:

- 80 mL of feedstock is charged to the round bottom flask.
- The flask has been placed in the heating mantle stirrer and connected to the air tube and condenser. It is confirmed that the cooling water is flowing through the condenser to prevent any evaporation of the light gas oil. A thermometer is inserted to measure the reaction temperature.
- When the required temperature is achieved, 0.8 g of the prepared catalyst is added to the reactor with a compressor operation and the time is recorded.

- At the end of the run, the heating mantle stirrer is turned off and the product material is filtered.
- The reactor is washed, drying the process and prepare to start the next run.
- All products are tested for sulfur content.

2.3.3. Adsorption of oxidized sulfur

The adsorption process between catalyst and sulfur compounds includes the contact of sulfur compounds that have low negative charge on the surface of catalyst having low positive charge and forming a polar interaction with the surface of catalyst where the oxidation reactions occur. So that, oxidation process increases the polarity of the oxidized sulfur compounds leading to increase the selectivity of sulfur compounds toward adsorption process due to such polarity [37].

2.4. Analysis of liquid samples

The sulfur content in the feedstock and products has been tested in laboratory of oil and its derivatives- Erbil/Iraq. Product sulfur content is analyzed by X-ray fluorescence following the ASTM D4294 method.

3. Mathematical model of batch reactor for ODS reaction

Mathematical modeling is the art of translating problems from an application area into tractable mathematical formulations whose theoretical and numerical analysis provides insight, answers, and guidance useful for the originating application [38]. The model used in this study is composed by a set of equations taken from literature while the kinetic parameters are estimated by reducing the sum of the squared error between experimental data and model prediction. The gPROMS (general Process Modeling System program) is used for modeling, simulation and optimization of ODS process based on the prepared catalyst [39].

3.1. Mass balance equations

Mass balance equation of batch reactor for ODS process is composed of several differential and algebraic equations. The general mass balance over catalytic batch reactor in total sulfur compound inside reactor is

Accumulation=Input-Output±Generation or disappearance by chemical reaction (4)

Input= Output = 0 (in the batch reactor) (5)

$$\text{Accumulation of sulfur} = \mathrm{V}.\frac{\mathrm{dC_{sulfur}}}{\mathrm{dt}} \quad (6)$$

$$\text{Disappearance of sulfur by the reaction} = \mathrm{V}.(-\mathrm{r_{sulfur}}) \quad (7)$$

Substitution of Eq. (5) into Eq. (4) giving the following eq.

Accumulation= Disappearance by reaction (8)

From Equations (6 to 8)

$$\frac{\mathrm{d_{sulfur}}}{\mathrm{dt}} = (-\mathrm{r_{sulfur}}) \quad (9)$$

$$\mathrm{dt} = \frac{\mathrm{d_{sulfur}}}{(-\mathrm{r_{sulfur}})} \quad (10)$$

where: at t=0 $C_{sulfur} = C_{sulfur,t}$; at t=t $C_{sulfur} = C_{sulfur}$.

By integration:

$$\mathrm{t} = \int_{\mathrm{C_{sulfur,t}}}^{\mathrm{C_{sulfur}}} \frac{\mathrm{d_{sulfur}}}{(-\mathrm{r_{sulfur}})} \quad (11)$$

3.2. Chemical reaction rate

The mechanism and the kinetic of catalytic air oxidation of sulfur are complex involving many steps to reach the end of reaction. The complexity of the chemical reaction could be taken into account by assuming nth order kinetics.

$$(-r_{sulfur}) = K_{app} {C_{sulfur}}^{n} \quad (12)$$

The apparent kinetic constant (k_{app}) is associated to intrinsic kinetic constant by internal diffusion that is represented by the catalyst effectiveness factor (η_0) [40]. So that, the reaction rate equation can be presented as follow:

$$(-r_{sulfur}) = \eta_0 \, k \, {C_{sulfur}}^{n} \quad (13)$$

The reaction rate constant is influenced by the temperature according to (Arrhenius equation) [41-42].

$$k=k_0 e^{(-\frac{EA}{RT})} \quad (14)$$

From equation (13 and 14),

$$(-r_{sulfur}) = \eta_0\, k_o e^{(\frac{-EA}{RT})}\, {C_{sulfur}}^n \quad (15)$$

Also, k_o and EA can be calculated by linearization of equation 14, which gives the following equation:

$$lnk = lnk_o - (\frac{-EA}{R}\frac{1}{T}) \quad (16)$$

By substitute equation 13 in equation 11 and integration these equation, the final expression of the catalytic oxidation reaction of sulfur with n^{th} order kinetic can be presented as follows:

$$C_{sulfur} = [\, {C_{sulfur,t}}^{(1-n)} + (n-1).t.K_{app}]^{(\frac{1}{1-n})} \quad (17)$$

3.3. Reactor performance

The oxidation reaction of the sulfur compound present in light gas oil is carried out in the batch reactor. The process includes number of parameters mainly, diffusivities, effectiveness factors, oil viscosity and others. These parameters are determined by using the correlations presented in this chapter.

$$K_{app} = \eta_0\, K_{in} \quad (18)$$

Hence, equation 17 is written as follows:

$$C_{sulfur} = [\, {C_{sulfur,t}}^{(1-n)} + (n-1).t.K_{in}.\eta_0]^{(\frac{1}{1-n})} \quad (19)$$

3.3.1. Effectiveness factor (η_0)

The effectiveness factor (η_0) can be determined as function of Thiele modulus with the following equation valid for sphere particles [43-44].

$$\eta_0 = \frac{3(\phi\, \coth\phi - 1)}{\phi^2} \quad (20)$$

While, the generalized Thiele modulus for nth-order irreversible reaction is determined by the following equation [43-44].

$$\phi = \frac{V_P}{S_P}\sqrt{(\frac{n+1}{2})\frac{k_{in}\, {C_{sulfur}}^{(1-n)}\rho_p}{D_{ei}}} \quad (21)$$

3.3.2. The effective diffusivity (D_{ei})

The effective diffusivity of the catalyst structure (porosity and tortuosity) is represented by taking the pores network inside the particle into account as follows [40,44].

$$D_{ei} = \frac{\varepsilon_B}{\mathcal{T}}\frac{1}{\frac{1}{D_{mi}}+\frac{1}{D_{ki}}} \quad (22)$$

where, catalyst porosity (ε_B) can be calculated by the following two equations based on experimental data:

$$\varepsilon_B = V_g \rho_p \quad (23)$$

$$\rho_p = \frac{\rho_B}{1-\varepsilon_B} \quad (24)$$

The tortuosity factor ($\mathcal{T}$) of the pore network have the value of (2 to 7)[45]. According to literatures, the tortuosity factor has reported to be 4 [40-43]. The effective diffusivity within the catalyst particle contains two types of diffusivity, Knudsen diffusivity D_{ki} and molecular diffusivity D_{mi}.

The Knudsen diffusivity is calculated as follows [40,43]:

$$D_{ki} = 9700\, r_g (\frac{T}{M_w})^{0.5} \quad (25)$$

where, mean pore radius (r_g) is estimated from this equation [46]:

$$r_g = \frac{2V_g}{S_g} \quad (26)$$

The molecular diffusivity is calculated by Tyn-Calus equation [47-48]:

$$D_{mi} = 8.93 * 10^{-8} (\frac{{v_l}^{0.267} T}{{v_s}^{0.433}\mu_l}) \quad (27)$$

3.3.3. Molar volume

The molar volume of the model sulfur compound is calculated by the following equation [48]:

$$v_{sulfur} = 0.285(v_{csulfur})^{1.048} \quad (28)$$

$$v_l = 0.285(v_{cl})^{1.048} \quad (29)$$

$$v_{cl} = (7.5214 * 10^{-3}(T_{meABP})^{0.2896}(\rho_{L15.6})^{-0.7666})Mw_L \quad (30)$$

The critical volume of liquid (light gas oil) is estimated by a Riazi–Daubert correlation [49]:

3.3.4. External volume(V_p) and surface (S_p) of the catalyst

The external volume (V_p) and external surface (S_p) of the catalyst can be calculated according to shape of the particle; for sphere particle:

$$V_p = \frac{4}{3}\pi(r_p)^3 \quad (31)$$

$$S_p = 4\pi(r_p)^2 \quad (32)$$

3.3.5. Viscosity(μ_l)

The viscosity of light gas oil can be calculated by using Glaso's equation as follows [50]:

$$\mu_l = 3.141 * 10^{10}(T - 460)^{-3.444}(logAPI)^{\alpha} \quad (33)$$

Where, (α) is Dimensionless number and estimated from this equation:

$$\alpha = 10.313[log_{10}(T - 460)] - 36.447 \quad (34)$$

Also, American Petroleum Institute (API) is estimated from this equation:

$$\text{API} = \frac{141.5}{sp.gr_{15.6}} - 131.5 \quad (35)$$

The equations of the mathematical model in this chapter are encoded for the ODS interaction and solved using the gPROMS (general Process Modeling System) package.

4. Kinetic parameter estimation technique

Estimating the kinetic parameter is very important step in many fields of science and engineering when many physiochemical processes are described by the equations system containing unknown parameters. Recently, the benefits of developing kinetic models for chemical engineers have increased with accurate calculations of parameters due to advanced control techniques and optimization of process, which can apply the fundamental models.

The appropriate value of the kinetic parameters can be estimated by reducing the errors between experimental data and predicted data by the mathematical model. Therefore, the predicted values from the model should match the experimental data as closely as possible [51]. For the purpose of optimizing the process, reactor design, process control and catalyst selection, it is important to develop kinetic models that can accurately predict the concentration of the product under the conditions of the process.

In this study, the best values of the kinetic parameters of the relevant reactions are achieved by utilizing two approaches that depend on the sulfur content in the oxidation process under different operating conditions. These approaches are given below:

- **Linear regression**: Determines the reaction rate constant (k) and order of the interaction (n), then utilizing the Arrhenius equation with linear regression to evaluate the activation energy (EA) and pre-exponential factor (k_o).
- **Non-linear regression:** Evaluates the order of reaction (n), the pre-exponential factor (k_o) and activation energy (EA) directly.

In order to estimate the best value for the kinetic parameter, the following objective function was minimized as shown below:

$$\text{OBJ} = \sum_{n=1}^{Nt}\left(C_{sulfur}^{exp} - C_{sulfur}^{pred}\right)^2 \quad (36)$$

In equation (36), Nt,C_{sulfur}^{exp} and C_{sulfur}^{prd} represent the numbers of runs, the experimental concentration and predicted concentration by model of sulfur content respectively. The conversion of sulfur compound can be calculated using the following equation:

$$X_{sulfur} = 1 - \frac{C_{sulfur}}{C_{sulfur.t}} \quad (37)$$

4.1. Optimization problem formulation for parameter estimation

The formulation of optimization problem for parameter estimation can be stated as follows:
Given: The reactor configuration, the catalyst and the process conditions.
Obtain: For the first approach: The reaction orders of oxidation reaction (n) for the catalyst and reaction rate constant (k) at different temperature (363, 383, 403, 423) K respectively and then calculation the activation energy and pre-exponential factor by linear regression by Arrhenius equation. For the second approach: the reaction order (n), activation energy (EA) and pre-exponential factor (ko) are simultaneously estimated for the catalyst.
So as to minimize: The sum of squared error (SSE).
Subjected to: Constraints on the conversion and linear bounds on all optimization variables Mathematically using linear regression, the optimization problem can be presented as follow:

Min: **SSE**

$n, k_i, (i = 1 - 4)$

S.t.f(z, x(z),ẋ(z), u(z),v) = 0

$C_L \leq C \leq C_U$

$n_l \leq n \leq n_u$

$k_{iL} \leq k_i \leq k_{iU}$

While by using the second approached (nonlinear regression) the problem can be presented as follow:

Min: **SSE**

n, EA, k_0

S.t.f(z, x(z),ẋ(z), u(z),v) = 0

$C_L \leq C \leq C_U$

$n_l \leq n \leq n_u$

$EA_L \leq EA \leq EA_U$

$k_{OL} \leq k_i \leq k_{OU}$

S.t.f(z, x(z),ẋ(z), u(z),v) = 0: represent the process model that presented previously.
z: is independent variable; u(z): is the decision variable; x(z): represent the set of all variables; ẋ(z): represent the derivative of the variables with respect to time; v: is the design variable; C, C_L, C_U: concentration , lower and upper bounds of concentration; L, U: are lower and upper bounds.

The method of optimization solution by gPROMS is performed by two steps that can be presented as follows [52]:

- First, performs a simulation which converge all the equality constraints described by function (f) and also to satisfy the constraints of inequality.
- Secondly; performs the optimization (the values of the decision variables such as the kinetic parameters that can be updated).

5. Results and discussion

5.1. Catalyst characterization

5.1.1. Chemical composition

XRF is used to determine the structural formula of the prepared samples and the actual metal oxide loaded (Fe_2O_3). As shown in Table 3, the purity of the prepared γ-alumina is 97.8%. The chemical composition for the prepared catalyst are summarized in Table 4. A good percentage of the active metal appear is observed.

Table 3. XRF results of the prepared γ-alumina concentration

Compounds	Concentration
Al_2O_3	69.07
SiO_2	0.804
P_2O_5	0.508
SO_3	0.021
Other components	0.227
Sum of concentration	70.63

Table 4. Chemical composition of the prepared catalyst

Compounds	Concentration
γ-Al_2O_3	94.14
Fe_2O_3	4.117

5.1.2. X-ray diffraction (XRD)

Figure 5 shows the XRD pattern of synthesized nano γ–alumina powder prepared. The three main reflections of nano γ-Al_2O_3 phase are obviously observed as broad peaks at 2θ angles around (36.8263º, 45.8903º, and 66.6322º), respectively [53-55]. The peaks in the pattern are significantly indicated that the formation of nano sized γ-Al_2O_3 crystallites is obtained. The size of crystallites was correlated using Scherrer's equation [56] as follows.

$$d = 0.94\lambda/\beta \cos \theta \quad (38)$$

where d is the diameter of crystallite; λ is the X-ray wave length; β is the broadening line at the half maximum intensity which represents the full width at half maximum (FWHM); θ is the Bragg angle at which the scattering wave was reflected or scattered at lattice plane producing intense peaks.

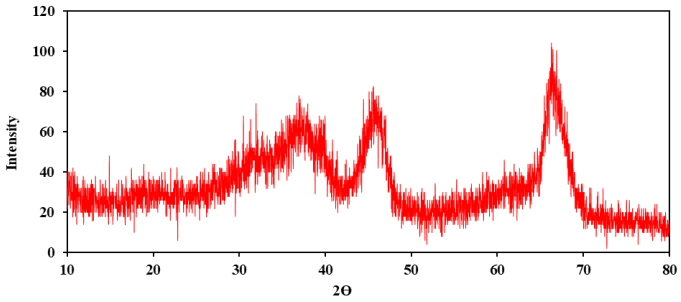

Figure 5. XRD patterns for synthesized nano γ–alumina powder

The average diameter of crystallite is 27.32 nm for the prepared nano γ–alumina powder. The percent crystallinity of samples is ascertained by comparing the ratio of intensity of the peaks for the prepared γ-alumina with the corresponding ratios of standard γ-alumina sample [57].

Table 5. characteristic peaks and their relative intensities for prepared nano γ–alumina powder

2θ	intensity I	intensity I standard
66.6322	100	100
45.8903	83	80
37.7555	27	65

Therefore, crystallinity % is determined as follows [52]:

$$\text{Crystallinity } \% = \frac{\Sigma \text{ I sample}}{\Sigma \text{ I refrence}} \quad (39)$$

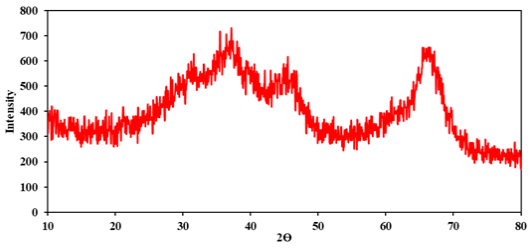

Figure 6. XRD patterns for the prepared catalyst

The percent crystallinity is estimated to be 85.7% for prepared nano γ–alumina powder. The crystallinity is considered to be one of the most important effected factors on thermal stability, where, thermal stability is increased with increasing the crystallinity [58-59]. Figure 6 shows the XRD patterns of the prepared catalyst after calcination at 550°C. The diffractogram of commercial iron oxide shows the characteristic peaks of Fe_2O_3 at 33.2º, 35.6º, 49.4º, 54.1º, 62.4º and 63.9º [60].

When impregnated with Fe_2O_3 in the catalyst, it is seen that the intensity of the peaks corresponding to γ-alumina drops, and the peaks corresponding to Fe_2O_3 start appearing as shown in the Figure 6.

5.1.3. Surface area and pore volume analysis

The surface area, pore volume and pore size of synthesized support and catalyst are summarized in Table 6. It can be observed that after impregnation, pore volume and the surface area decreased slightly due to the occupation of the active component in some spaces within the samples. Also, The bulk density is 0.482 gm/cm^3 for the prepared catalyst.

Table 6. Summary of surface area, pore volume and pore size of the prepared γ-alumina and catalyst

Compounds	γ-alumina	Fe_2O_3/γ-alumina
Surface area (BET), m^2/g	263.91	256.68
Pore volume, cm3/g	0.3163	0.316
Pore size, nm	4.79419	4.92913

5.1.4. Fourier transform infrared (FTIR)

FTIR analysis for the synthesized γ-alumina in the wave number region of 4000-500 cm-1 are shown in Figure 7. The band located at 3412 cm^{-1} was attributed to the O–H stretching vibration and the band at ~1650 cm^{-1} was related to the H–O–H symmetric stretching vibration of adsorbed water molecules. The absorption bands centered at 650 attributed to stretching vibrations of Al-O, which is characteristic of γ-alumina as shown in Figure 7 [61-63]. Figure 8 shows the FTIR spectra of the synthesized nano catalyst after loading of Fe_2O_3. Based on the results presented in Figure 7 and 8, there is no difference in the wave number regions before and after loading. Such good results indicated that there is no chemical change in the composition of the support after loading process. Also, no bonds of iron oxides were found resulting that there is insufficient amount of iron oxide to give the peaks.

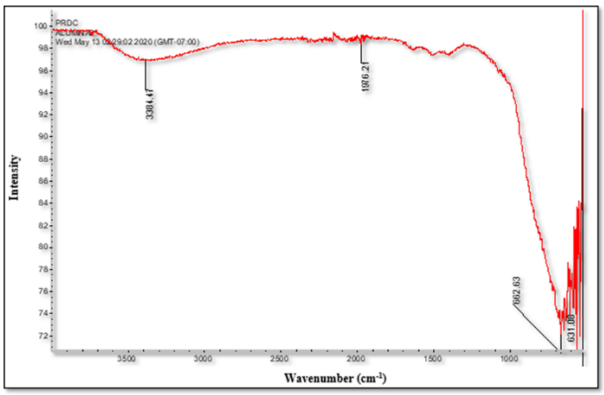

Figure 7. FTIR for synthesized γ-alumina

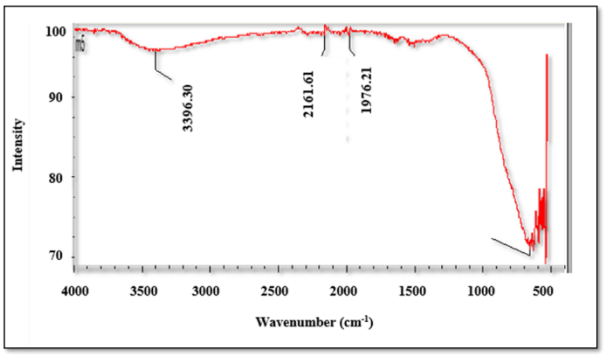

Figure 8. FTIR for synthesized catalyst

5.1.5. Thermal gravimetric analysis (TGA)

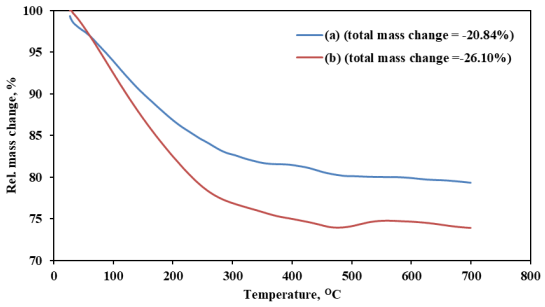

Figure 9. TGA of synthesized (a) nano γ–alumina, (b) catalyst

Figure 9 shows the TGA profiles of the prepared γ-alumina and catalyst samples. From this Figure, there are two regions of mass loss where, the first one, (between 20-120°C), with mass loss values around 10 %, is related to the evaporation of physically adsorbed water on the solid [64-65]. In the range of 180-350°C, it comes from the release of the chemisorbed water, which takes place around 250°C [66]. At temperatures above 450°C, the weight of all samples tends to remain stable. The mass loss values observed

in the TGA experiments is -20.84% for the prepared γ-alumina and -26.10% for the catalyst. Such good results indicated that the support and prepared catalyst have a good thermal stability.

5.1.6. Particle size distribution

Figures 10 shows the particle distribution of the prepared catalyst. The average nano particle size is 84.65 nm and the overall range of the diameters between 55 - 135 nm. Maximum volume percentage of the particles is 23.76 % at size distribution of 90 nm, and minimum volume percentage is 1.03 % for particles at size of 130 nm.

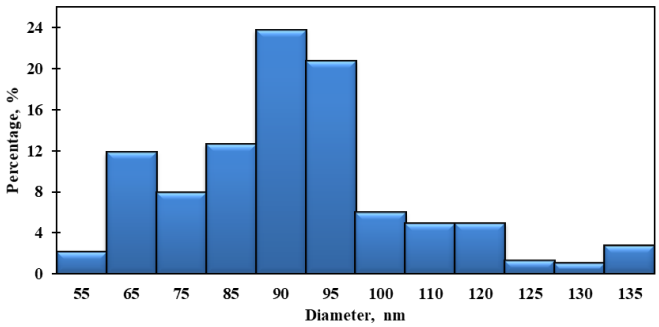

Figure 10. Granularity accumulation distribution of the synthesized catalyst

5.1.7. Scanning Electron Microscopy (SEM)

As shown in Figure 11, the SEM of the catalyst showed that the particle size is <100 nm. Also, the shape of the particles that are presented in these Figure are in the spherical form.

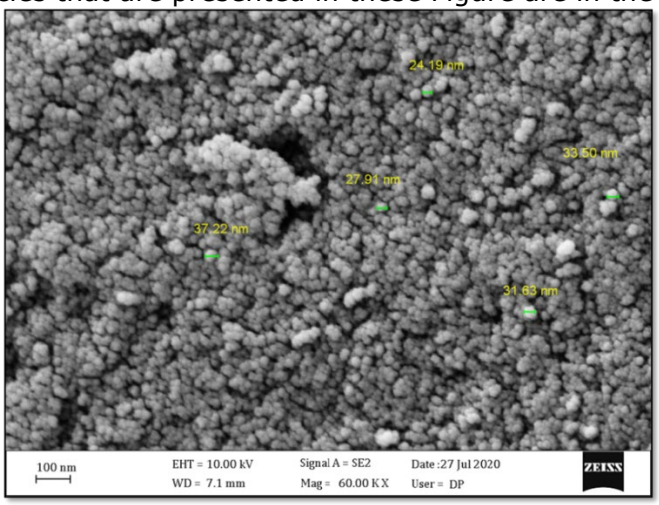

Figure 11. SEM images of the synthesized catalyst

5.2. Oxidative desulfurization results

The oxidative desulfurization process is employed to test the activity of the prepared catalyst. Light gas oil (LGO) is used as an oil feedstock and air as an oxidant in a batch reactor. Several operating conditions affecting the reduction of sulfur content such as reaction time and reaction temperature are studied.

5.2.1. Effect of reaction temperature

The impact of the reaction temperature on the sulfur removal in ODS reactions has studied at 363 K, 383 K,403 K and 423 K, and the results are illustrate in Figure 12.

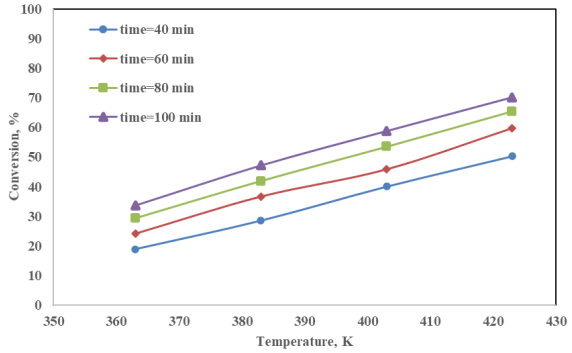

Figure 12. Temperature influence of sulfur removal for the prepared catalyst at various reaction time

It can be observed from Figure 12 above that increasing the reaction temperature leads to increase the conversion of sulfur compound. Such attitude is due to the fact that the temperature affect positively the reaction rate constant (rate constant) leading to an increase in the sulfur compound conversion [67] according to Arrhenius equation. So, increasing the temperature causes an increase in the number of molecules having activation energy and thus an increase in the number of molecules involved in the oxidation reaction resulting in an increase in conversion.

Also, the catalyst activities is highly affected by the calcination temperatures. The density of acid sites is strongly influenced by the catalyst calcination temperature; it is increased to reach a maximum that leads to enhance the removal of sulfur compound from diesel fuel. The optimum temperature for γ-Al_2O_3 powder synthesized by flash calcination is 650°C that surface area and pore volume are maximized [68]. So, this study was used the calcination temperature of 650°C to prepare γ-Al_2O_3 for achieving high catalytic activity in ODS process.

5.2.2. Effect of reaction time

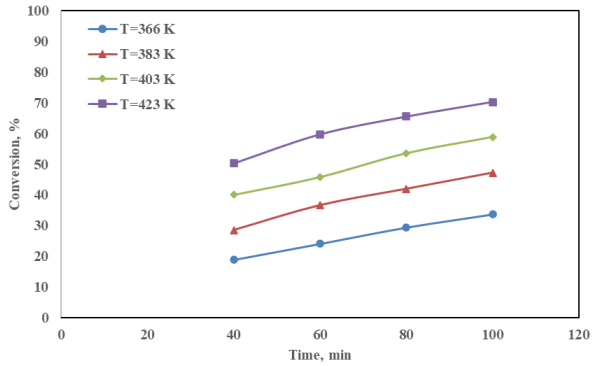

Figure 13. Time influence of sulfur removal for the prepared catalyst at various reaction temperature

The impact of the reaction time on the removal of sulfur compound by oxidation reaction has investigated at 40 min, 60 min, 80 min and 100 min, which are illustrated in Figure 13. In general, the results showed that an increase in the desulfurization efficiency with the reaction time. Where, increasing the time of the reaction offers the chance for the reactants to contact then to react among them. As a result, the contact time among the reactants increases giving longer contact with the active site of the catalyst [69].In Figure 13, the conversion of sulfur compound increased from 50.33% to 70.29% when the reaction time increases from 40 min to 100 min at 423 K.

5.3. Kinetic parameters estimation

The optimal kinetic parameters can be estimated using a mathematical model aimed at minimizing the error between the experimental data and the predicted data by the mathematical model to get predicted values from model as close as possible to the experimental data [70]. The constant parameters used in the mathematical model are shown in Table 7.

Table 7. Values of constant parameters used in ODS model

Parameter	Symbol	Unit	Value
Initial concentration	Ct	wt%	0.751
Time	Time1, time2, time3, time4	min	time1=40, time2=60, time3=80, time4=100
Temperature	T1, T2, T3, T4	K	T1=363, T2=383, T3=403, T4=423
Density of light gas oil at 15.5°C	ρ_l	gm/cm^3	0.8205
Mean average boiling point	T_{meABP}	°R	957

Parameter	Symbol	Unit	Value
Acceleration gravity	g	m/sec^2	9.81
Gas constant	R	J/mole.°K	8.314
Pore volume per unit mass of catalyst	Vg	cm^3/gm	0.316
Specific surface area of particle	Sg	cm^2/gm	2566800
Volume of catalyst particle	Vp	cm^3	$3.1759*10^{-16}$
External surface area of particle	Sp	cm^2	$2.25114*10^{-10}$
Bulk density	ρ_B	gm/cm^3	0.482
Molecular weight of light gas oil	M_{wL}	gm/mole	200.468
Molecular weight of sulfur	Mwi	gm/mole	32.06
Mean pore radius	r_g	nm	2.4645

5.3.1. Linear regression

The optimal results of the model parameters obtained by linear approach are reported in Table 8 below for the catalyst:

Table 8: Optimal model parameters obtained by optimization process using linear approach

Parameter	Value	Unit
n	1.9133123	_
k1	0.00674264	$(wt^{-0.9133123}).min^{-1}$
k2	0.01183655	$(wt^{-0.9133123}).min^{-1}$
k3	0.01921438	$(wt^{-0.9133123}).min^{-1}$
k4	0.02902299	$(wt^{-0.9133123}).min^{-1}$
SSE	1.802865×10^{-3}	_

Activation energy

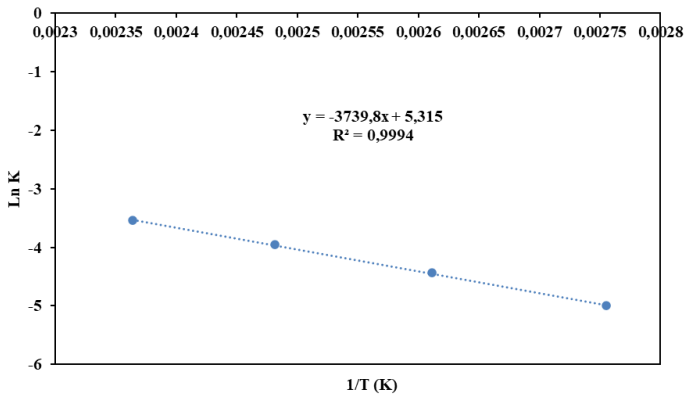

Figure 14. (ln k) versus (1/T) for kinetic parameters of the oxidation process

According to Arrhenius equation, a plot of (lnk) versus (1/T) gives a straight line with slope equal to (-EA/R) in which the activation energy is calculated as illustrated in Figure 14.

The activation energy and pre-exponential factor which can be obtained from this Figure is 31.093 kJ/mol and 203.365, respectively.

5.3.2. Non-linear regression

In this approach, pre-exponential factor, the activation energy, and interaction order, have simultaneously been estimated and the values of these parameters are shown in Table 9.

Table 9. Optimal kinetic model parameters obtained via optimization process by non-linear approach

Parameter	Value	Unit
n	2	_
EA	34.305	KJ/mol.
k_o	578.64	$wt^{-1}.min^{-1}$
SSE	1.712543×10^{-3}	_

5.4. Experimental and simulation results

The gPROMS software is used for the simulation of the process. The experimental and predicted results are summarized in Tables 10 and 11 below, and also illustrated in Figure 15 (for non-leaner approach).

Table 10. Experimental and simulation results using linear approach

Temperature (K)	Time (min)	Sulfur content (wt %)		Conversion		Error %
		Experimental	Predicted	Experimental	Predicted	
363	40	0.610	0.621	0.188	0.173	1.85
363	60	0.571	0.571	0.240	0.240	0.06
363	80	0.531	0.528	0.293	0.297	0.49
363	100	0.499	0.491	0.336	0.346	1.50
383	40	0.537	0.548	0.285	0.270	2.10
383	60	0.476	0.482	0.366	0.358	1.23
383	80	0.436	0.429	0.419	0.428	1.53
383	100	0.397	0.387	0.472	0.485	2.49
403	40	0.450	0.468	0.400	0.377	3.91
403	60	0.407	0.392	0.458	0.478	3.63
403	80	0.349	0.337	0.536	0.552	3.46
403	100	0.309	0.295	0.589	0.608	4.69
423	40	0.373	0.391	0.503	0.480	4.74
423	60	0.302	0.133	0.598	0.823	3.58
423	80	0.259	0.260	0.655	0.654	0.54
423	100	0.223	0.222	0.703	0.704	0.40

Table 11. Experimental and simulation results using non-linear approach

Temperature (K)	Time (min)	Sulfur content (wt %)		Conversion		Error %
		Experimental	Predicted	Experimental	Predicted	
363	40	0.610	0.625	0.188	0.168	2.55
363	60	0.571	0.577	0.240	0.232	1.11
363	80	0.531	0.536	0.293	0.287	0.92
363	100	0.499	0.500	0.336	0.335	0.25
383	40	0.537	0.551	0.285	0.267	2.52
383	60	0.476	0.486	0.366	0.353	2.02
383	80	0.436	0.435	0.419	0.421	0.34
383	100	0.397	0.393	0.472	0.477	0.90
403	40	0.450	0.463	0.400	0.383	2.85
403	60	0.407	0.389	0.458	0.483	4.46
403	80	0.349	0.335	0.536	0.554	3.98
403	100	0.309	0.294	0.589	0.609	4.83
423	40	0.373	0.374	0.503	0.502	0.24
423	60	0.302	0.299	0.598	0.602	1.07
423	80	0.259	0.249	0.655	0.669	3.82
423	100	0.223	0.213	0.703	0.716	4.41

The sums of squared errors (SSE) is 0.0018 and 0.0017of linear approach and nonlinear approach respectively. So, the parameter estimated by the nonlinear approach is more accurate than those calculated by the linear approach. The values of the activation energy (EA) and pre-exponential factor (k_o) estimated via linearization (linear approach) of Arrhenius equation gives high error as compared with those estimated via non-linear method (nonlinear approach).

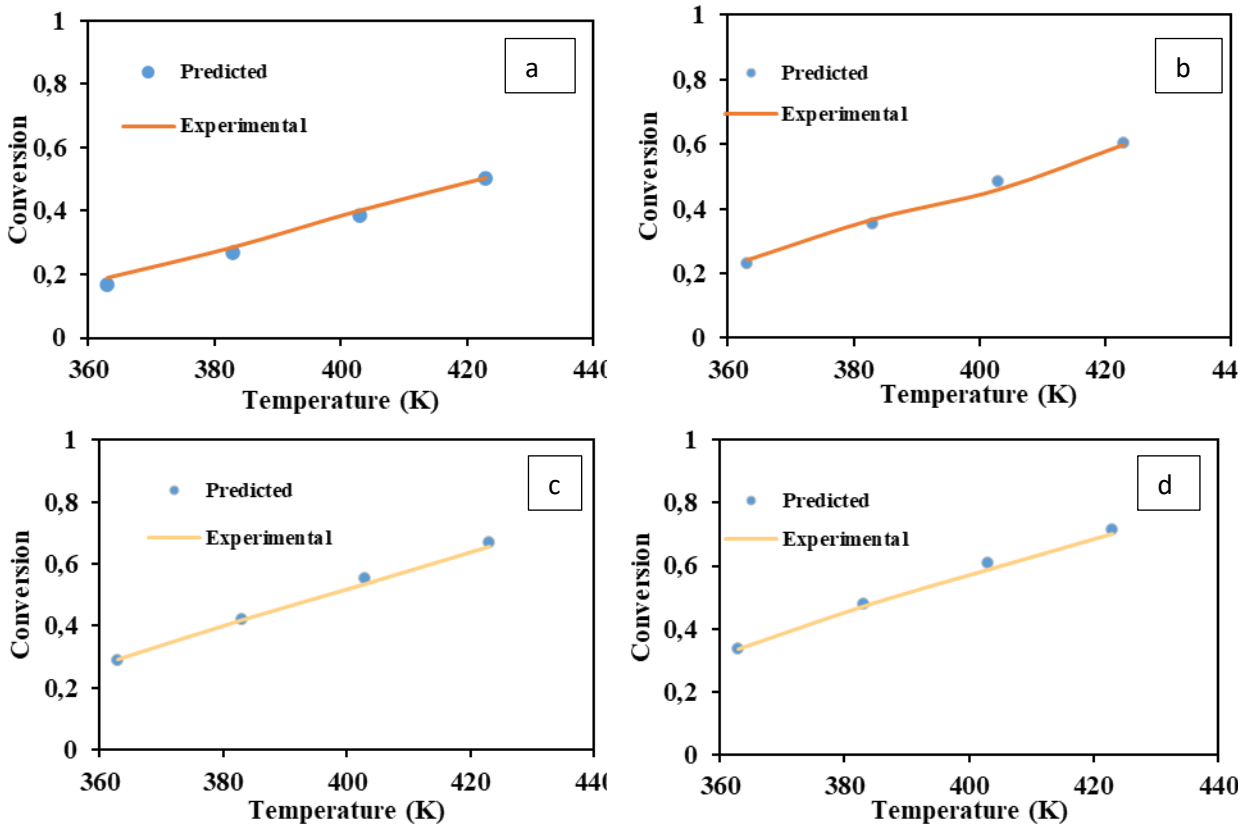

Figure 15. Comparison between experimental and simulated data at (a) 40 min (b) 60 min (c) 80 min (d) 100 min

From these results, it is observed that increasing the reaction temperature and reaction time increases the reaction rate of ODS process based on the following points.

- **Temperature:** Increasing the reaction temperature leads to increase the conversion of sulfur compound due to the reaction rate constant that is influenced by the temperature. Where, the temperature is dependent by Arrhenius equation leading to an increase in the sulfur compound conversion. Also, rising the reaction temperature contributes in an increasing of magnitudes of some important physical properties such as diffusivity, viscosity and surface tension. Thus, the rate of absorption of molecular air into light gas oil and the diffusing rate of the sulfur compound beside the rate of dissolving air inside the pores of the catalyst to reach the active sites increases with increasing the reaction temperature.
- **Time:** The rise in the reaction time will increase the contact time among the reactants on the active sites of catalyst. So, high residence time is achieved giving high reaction.

6. Optimal operation conditions for maximum conversion of ODS process

6.1. Optimization problem formulation for maximum conversion

Based on the experiments and after obtaining the optimal kinetic parameter for the ODS process, the optimal operating conditions for obtaining the minimum sulfur content are necessary. Therefore, the optimization problem can be formulated for the maximum conversion of the process as follows:

Given: The reactor configuration, the reaction order, the catalyst and pre-exponential factor and activation energy for the reaction.

Obtain: The best operating conditions for high conversion.

So as to minimize: The sulfur concentration.

Subjected to: Process constraints and linear bounds on all optimization variables in the process.

Mathematically, the problem can be represented as follows:

Min: C_{sulfur}

$T, time_i, C_{sulfur}$

S.t. f(z, x(z),ẋ(z), u(z),v) = 0

$time_L \leq time \leq time_U$

$C_{sulfur.tL} \leq C_{sulfur.t} \leq C_{sulfur.tU}$

$T_L \leq T \leq T_U$

$X_{sulfur.tL} \leq X_{sulfur.t} \leq X_{sulfur.tU}$

The optimization solution method is performed by gPROMS software.

6.2. Optimal operating conditions for maximum conversion

After obtaining the optimal kinetic parameters, such optimal values will be used in the kinetic model in order to obtain the best operating conditions to give the minimum sulfur content in the products based on the prepared catalyst achieving the main goal of this study, which is an environmentally friendly fuel. The optimal values of the operating conditions for the prepared catalyst are presented in Table 12.

Table 12. Optimal operating conditions for ODS process

Parameter	Value	Unit
$C_{sulfur.t}$	0.757	wt%
T	550	K
Time	200	min
Conversion	97.97	%

The sulfur content in the petroleum products has been reduced by finding the optimal operating conditions to achieve the environmental and industrial aspects demands .As can be seen from the presented results in Table 12, the maximum sulfur removal (higher than 97%) has been achieved at the reaction temperature of 550 K, contact time at 200 min and initial concentration of sulfur compound at 0.757 ppm to match the environmental regulations to get almost free sulfur content and as a result high fuel oil quality.

7. Conclusions

In this study, the homemade nano catalyst (Fe_2O_3/γ-Al_2O_3 nanoparticles) is successfully applied for ODS process using air as oxidant in batch reactor. The nano-gamma alumina is prepared by precipitation method and then the impregnation method is used to generate the catalyst. The method of impregnation is a good method in preparing the nano catalyst because it gives a good distribution of the active metals in addition to the high surface area and the distribution of pore for prepared catalyst. Several characterization tests such as SEM, XRD, XRF, TGA, FTIR, BET and particle size distribution were conducted on the prepared γ-Al_2O_3 and the prepared catalyst. Such tests indicated that γ-Al_2O_3 produced by precipitation method has high purity, high surface area and high crystallinity. Also, a good distribution of active metal (Fe), various surface morphology and high dispersion of active metal were obtained. As well as, the result of the particle size distribution test for the prepared nano-catalyst indicated that the particle size of the catalyst is reported to be < 100 nm. The experimental conversion of sulfur compounds presented in real light gas oil has (70.29%) under the conditions of temperature = 423 K and reaction time = 100 min. The simulation and optimization techniques are applied in this study to estimate the optimal kinetic parameter based on experimental results. Estimation of these parameters is conducted by minimizing the sum of squared error between experimental and predicted results and all results gave absolute error less than 5% at different conditions. The simulation and optimization techniques are achieved using two approaches (linear and non-linear method) and the simulation results show that the non-linear approach is more accurate due to it give less (SSE) in comparison with linear approach. The optimal kinetic parameters can be used to estimate the optimal operating conditions to achieve

cleaner fuel with sulfur conversion above 97% at process temperature= 550 °K, batch time=200 min and initial concentration = 0.7574 wt%."

Nomenclature

C_{sulfur}	Sulfur Concentration
X_{sulfur}	Conversion of sulfur compound.
C_{sulfur}	Concentration of sulfur compound at the end of the reaction.
$C_{sulfur.t}$	Initial concentration of sulfur present in light gas oil.
k	Reaction Rate Constant
k_{App}	Apparent Rate Constant
$\mathcal{D}_{ei}$	Effective diffusivity
$\mathcal{D}_{ki}$	Knudsen diffusivity
$\mathcal{D}_{mi}$	Molecular diffusivity
$Sp.gr_{15.6}$	Specific gravity of of light gas oil at 15.6°C
EA	Activation Energy
Mw_L	Liquid molecular weight of
Mw	Molecular weight of sulfur
R	Gas constant
n	Order of reaction
$-r_{sulfur}$	Reaction rate of sulfur
r_g	Pore radius (nm)
r_p	Particle radius
S_p	External surface area of catalyst particle
S_g	Specific surface area of particle
V_p	External Volume of catalyst particle
V_g	Pore volume
T_{meABP}	Mean average boiling point

Greek symbols

η_0	Effectiveness factor
Φ	Thiel modulus
$\mathcal{E}_B$	Porosity
$\mathcal{T}$	Tortuosity
ρ_B	Bulk density
ρ_p	Particle density
$\rho_{L15.6}$	Density of light gas oil at 15.6°C(gm/cm^3).
μ_l	Viscosity of liquid
v_l	Liquid molar volume
v_{cl}	Critical molar volume of liquid
v_{Sulfur}	Molar volume of sulfur
$v_{csulfur}$	Critical volume of sulfur compound.
^{o}	Initial (at time = 0)

Acknowledgment

The authors thank Petroleum Research and Development Center, The Iraqi Ministry of Oil /Baghdad, IRAQ for its financial support.

References

[1] Lelieveld J, Roelofs J, Ganzeveld L, Feichter J, Rodhe H. Terrestrial sources and distribution of atmospheric sulphur. Philosophical Transactions of the Royal Society of London. Series B: Biological Sciences, 1997; 352: 149-158.

[2] Farouq SM, Omar UA, Talal A, Yahya A, Inas MA. Deep oxidative desulfurization of liquid fuels. Reviews in Chemical Engineering, 2014; 30: 337-378.

[3] Nehlsen JP. Developing clean fuels: Novel techniques for desulfurization: Princeton University Princeton 2006, NJ.

[4] Gokhale S, Khare M. A review of deterministic, stochastic and hybrid vehicular exhaust emission models. International Journal of Transport Management, 2004; 2: 59-74.

[5] Zhao D, Sun F, Zhou E, Liu Y. A review of desulfurization of light oil based on selective oxidation. China: College of Chemistry and Pharmaceutical Engineering, 2003; 6: 17.
[6] Zongxuan J, LÜ H, Yongna Z, LI C. Oxidative desulfurization of fuel oils. Chinese journal of catalysis, 2011; 32: 707-715.
[7] Abdullah AA, Tawfik AS, Saheed AG, Mohammad NS, Khalid RA. Preparation of activated carbon, zinc oxide and nickel oxide composites for potential application in the desulfurization of model diesel fuels. Journal of Analytical and Applied Pyrolysis, 12017; 28: 246-256.
[8] Muhammad NH, Hoon CP, Hang SC. A comprehensive review on catalytic oxidative desulfurization of liquid fuel oil. Catalysts,2019; 9: 229.
[9] Song C, Ma X. New design approaches to ultra-clean diesel fuels by deep desulfurization and deep dearomatization. Applied Catalysis B: Environmental, 2003; 41: 207-238.
[10] Babich I, Moulijn J. Science and technology of novel processes for deep desulfurization of oil refinery streams: a review. Fuel, 2003; 82: 607-631.
[11] Muhammad NH, Hoon CP, Hang SC. A comprehensive review on catalytic oxidative desulfurization of liquid fuel oil. Catalysts, 2019; 9: 229.
[12] Xiaoliang M, Kinya S, Isao M. Hydrodesulfurization reactivities of various sulfur compounds in diesel fuel. Industrial & engineering chemistry research, 1994; 33: 218-222.
[13] Shujiro O, Takeshi N, Noriko T, Weihua Q, Atsushi I, Tamotsu I, Toshiaki K. Oxidative desulfurization of light gas oil and vacuum gas oil by oxidation and solvent extraction. Energy & fuels, 2020; 14: 1232-1239.
[14] Jeong KE, Tae WK, Joo WK, Ho JC, Chul UK, Young KP, Soon YJ. Selective oxidation of refractory sulfur compounds for the production of low sulfur transportation fuel. Korean Journal of Chemical Engineering, 2013; 30: 509-517.
[15] Bhasarkar JB, Dikshit PK, Moholkar VS. Ultrasound assisted biodesulfurization of liquid fuel using free and immobilized cells of Rhodococcus rhodochrous MTCC 3552: A mechanistic investigation. Bioresource technology, 2015; 187: 369-378.
[16] Wenshuai Z, Yehai X, Huaming L, Bilian D, Hu, X, Chao W, Yanhong C, Hui L. Photocatalytic oxidative desulfurization of dibenzothiophene catalyzed by amorphous TiO_2 in ionic liquid. Korean Journal of Chemical Engineering, 2014; 31: 211-217.
[17] Wan AW, Rusmidah A, Abdul Aziz A, Wan NA. The role of molybdenum oxide based catalysts on oxidative desulfurization of diesel fuel. Mod Chem Appl, 2015; 3: 1000150.
[18] Zhang G, Yu F, Wang R. Research advances in oxidative desulfurization technologies for the production of low sulfur fuel oils. Petroleum & Coal, 2009; 51: 196-207.
[19] Gao Y, Gao R, Zhang G, Zheng Y, Zhao J. Oxidative desulfurization of model fuel in the presence of molecular oxygen over polyoxometalate based catalysts supported on carbon nanotubes. Fuel, 2017; 224: 261-270.
[20] Zhang M, Zhu W, Xun S, Li H, Gu Q, Zhao Z, Wang Q. Deep oxidative desulfurization of dibenzothiophene with POMbased hybrid materials in ionic liquids. Chemical engineering journal, 2013; 220: 328-336.
[21] Yu FL, Liu CY, Yuan B, Xie CX, Yu ST. Self-assembly heteropoly acid catalyzed oxidative desulfurization of fuel with oxygen. Catalysis Communications, 2015; 68: 49-52.
[22] Rostami A, Navasi Y, Moradi D, Choghamarani AG. DABCO tribromide immobilized on magnetic nanoparticle as a recyclable catalyst for the chemoselective oxidation of sulfide using H2O2 under metal-and solvent-free conditions. Catalysis Communications, 2014; 43: 16-20.
[23] Teimouri A, Mahmoudsalehi M, Salavati H. Catalytic oxidative desulfurization of dibenzothiophene utilizing molybdenum and vanadium oxides supported on MCM-41. International Journal of Hydrogen Energy, 2018; 43: 14816-14833.
[24] Mokhtar NAW, Abu Bakar WAW, Abdullah WNW, Toeman S, Rosid SJM. Role of Mn/Al2O3 catalyst in deep oxidative desulfurization of diesel. Petroleum Science and Technology, 2018; 36: 1741-1747.
[25] Subhan S, Rahman AU, Yaseen M, Rashid HU, Ishaq M, Sahibzada M, Tong Z. Ultra-fast and highly efficient catalytic oxidative desulfurization of dibenzothiophene at ambient temperature over low Mn loaded Co-Mo/Al2O3 and Ni-Mo/Al2O3 catalysts using NaClO as oxidant. Fuel, 2019; 237: 793-805.
[26] Meman NM, Zarenezhad B, Rashidi A, Hajjar Z, Esmaeili E. Application of palladium supported on functionalized MWNTs for oxidative desulfurization of naphtha. Journal of Industrial and Engineering Chemistry, 2015; 22: 179-184.
[27] Toshima N, Yonezawa T. Bimetallic nanoparticles—novel materials for chemical and physical applications. New Journal of Chemistry, 1998; 22: 1179-1201.

[28] Liu H, Guan J, Mu X, Xu G, Wang X, Chen X. Nanocatalysis. Encyclopedia of Physical Organic Chemistry, 2016;1-75.
[29] Dorre E, Hubner H. Alumina: Processing, Properties and Applications.(Book). Springer-Verlag, 329, 1984.
[30] Lee J, Jeon H, Gun D, Szanyi J, HunKwak J. Morphology-dependent phase transformation of γ-Al2O3. Applied Catalysis A: General, 2015; 500: 58-68.
[31] Dionigi C, Ivanovska T, Liscio F, Milita S, Corticelli F, Ruani G. Fabrication and properties of non-isolating γ-alumina mesofoam. Journal of Alloys and Compounds, 666, 2016; 101-107.
[32] Teng X, Liu H, Huang C. Microstructures and mechanical properties of Al2O3/ZrO2 composite produced by combustion synthesis. Scripta Materialia, 2007; 53: 995-1000.
[33] Nazari S, Nazari S, Mansourizadeh F, Karimi G. Synthesis of Gamma-Alumina Nanopowders Using Waste Metal Aluminum and Stability Surfactants. International Journal of Nanoscience, 2019; 19: 1950014.
[34] Almeida TS, Caíque G, Silva RG, de Andrade AR. Addition of iron oxide to Pt-based catalyst to enhance the catalytic activity of ethanol electrooxidation. Journal of Electroanalytical Chemistry, 2017; 796: 49-56.
[35] Safaei M. Effect of temperature on the synthesis of active alumina by flash calcination of gibbsite. Journal of the Australian Ceramic Society, 2017; 53: 485-490.
[36] Asencios YJ, Sun-Kou MR. Synthesis of high-surface-area γ-Al2O3 from aluminum scrap and its use for the adsorption of metals: Pb (II), Cd (II) and Zn (II). Applied Surface Science, 258, 2012; 10002- 10011.
[37] Srivastava VC. An evaluation of desulfurization technologies for sulfur removal from liquid fuels. The royal society of chemistry, 2012; 2: 759-783.
[38] Neumaier A. Mathematical model building, in Modeling Languages in Mathematical Optimization. Springer, 2004; 37-43.
[39] Näf UG. Stochastic simulation using gPROMS. Computers & chemical engineering, 1994; 18: S743-S747.
[40] Nawaf AT, Jarullah AT, Abdulateef LT. Design of a Synthetic Zinc Oxide Catalyst over Nano-Alumina for Sulfur Removal by Air in a Batch Reactor. Bulletin of Chemical Reaction Engineering & Catalysis, 2019; 14: 79-92.
[41] Huang P, Luo G, Kang L, Zhu M, Dai B. Preparation, characterization and catalytic performance of HPW/aEVM catalyst on oxidative desulfurization. RSC advances, 2017; 7: 4681-4687.
[42] Saha B, Kumar S, Sengupta S. Green synthesis of nano silver on TiO2 catalyst for application in oxidation of thiophene. Chemical Engineering Science, 2019; 199: 332-341.
[43] Ghazwan SA, Jarullah AT, Al-Tabbakh B, Mujtaba IM. Design of An Environmentally Friendly Reactor for Naphtha Oxidative Desulfurization by Air Employing a new Synthetic Nano-Catalyst Based on Experiments and Modelling. Journal of Cleaner Production, 2020; 257: 120436.
[44] Jarullah AT, Ghazwan SA, Al-Tabbakh B, Mujtaba IM. Enhancement of Light Naphtha Quality and Environment using New Synthetic Nano-catalyst for Oxidative Desulfurization: Experiments and Process Modeling. Computers & Chemical Engineering, 2020; 140: 106869.
[45] Jarullah AT, Sarmad K, Al-Tabbakh B, Mujtaba IM. Enhancement of Light Naphtha Quality and Environment using New Synthetic Nano-catalyst for Oxidative Desulfurization: Experiments and Process Modeling. Chemical Engineering Research and Design, 2020;160: 405-416.
[46] Nawaf AT, Hamed HH, Hameed ShA, Jarullah AT, Mujtaba IM. Performance enhancement of adsorption desulfurization process via different new nano-catalysts using digital baffle batch reactor and mathematical modeling. Chemical Engineering Science, 2021; 232: 116384.
[47] Nawaf AT, Jarullah AT, Hameed ShA, Mujtaba IM. Design of new Activated Carbon based Adsorbents for Improved Desulfurization of Heavy Gas Oil: Experiments and Kinetic Modeling. Chemical Product and Process Modeling,2021; 16(3): 229-249.
[48] Jarullah AT, Sarmad K, Al-Tabbakh B, Mujtaba IM. Design of an environmentally friendly fuel based on a synthetic composite nano-catalyst through parameter estimation and process modelling. Chemical Product and Process Modeling, 2021; 17(3): 213-233.
[49] Ahmed T. Hydrocarbon phase behavior. Gulf Publishing: Houston 1989, TX; 424pp.
[50] Glaso O. (1980). Generalized Pressure-Volume-Temperature Correlations. Journal of Petroleum Technology, 1980; 32: 785-795.
[51] Poyton AA, Varziri MS, McAuley KB, McLellan PJ, Ramsay JO. Parameter estimation in continuous-time dynamic models using principal differential analysis. Computers & Chemical Engineering, 2006; 30: 698–708.

[52] Jarullah AT, Mujtaba IM, Wood AS. Kinetic model development and simulation of simultaneous hydro denitrogenation and hydrodemetallization of crude oil in trickle bed reactor. Fuel, 2011; 90: 2165- 2181.
[53] Hosseini SYG, Nikou MRK. Synthesis and characterization of different γ-Al_2O_3 nanocatalysts for methanol dehydration to dimethyl ether. International Journal of Chemical Reactor Engineering, 2012; 10.
[54] Khazaei A, Nazari S, Karimi G, Ghaderi E, Moradian KM, Bagherpor Z, Nazari S. Synthesis and characterization of γ-alumina porous nanoparticles from sodium aluminate liquor with two different surfactants. International Journal of Nanoscience and Nanotechnology, 2016; 12(4): 207-214.
[55] Sobhani M, Tavakoli H. The effect of cobalt addition on the meso-porous structured γ-Alumina synthesized by aqueous sol-gel method. Journal of Ultrafine Grained and Nanostructured Materials, 2019; 52: 84-89.
[56] Afruz FB, Tafreshi M. Synthesis of γ-Al_2O_3 nano particles by different combustion modes using ammonium carbonate, 2014; 52: 378-385.
[57] Rayalu SS, Udhoji JS, Meshram SU, Naidu RR, Devotta S. Estimation of crystallinity in fly ash-based zeolite-A using XRD and IR spectroscopy. Current Science, 2005; 89: 12.
[58] Król-Morkisz K, Pielichowska K. Thermal decomposition of polymer nanocomposites with functionalized nanoparticles, in Polymer Composites with Functionalized Nanoparticles. Elsevier, 2019; 405-435.
[59] Efrati R, Natan M, Pelah A, Haberer A, Banin E, Dotan A, Ophir A. The effect of polyethylene crystallinity and polarity on thermal stability and controlled release of essential oils in antimicrobial films. Journal of Applied Polymer Science, 2014; 13.
[60] Alvarez P, Araya P, Rojas R, Guerrero S, Aguila G. Activity of alumina supported Fe catalysts for N2O decomposition: effects of the iron content and thermal treatment. Journal of the Chilean Chemical Society, 2017; 62: 3752-3759.
[61] Sifontes ÁB, Gutierrez B, Mónaco A, Yanez A, Díaz Y, Méndez FJ, Llovera L, Cañizales E, Brito JL. Preparation of functionalized porous nano-γ-Al2O3 powders employing colophony extract. Biotechnology Reports, 2014; 4: 21-29.
[62] Saud A, Majdi HS, Saud S. Synthesis of nano-alumina powder via recrystallization of ammonium alum. Cerâmica, 2019; 65: 236-239.
[63] Hosseini SA, Niaei A, Salari D. Production of γ Al_2O_3 from Kaolin. Open Journal of Physical Chemistry, 2011; 1: 23-27.
[64] Álvaro-Muñoz T, Márquez-Álvarez C, Sastre E. Aluminium chloride: A new aluminium source to prepare SAPO-34 catalysts with enhanced stability in the MTO process. Applied Catalysis A: General,2014; 472, 72-79.
[65] YueMing Ch, MingKuang W, PanMing H, TsungMing T, KuoChuan L. Influence of catechin on precipitation of aluminum hydroxide. Geoderma, 2009; 152: 296-300.
[66] Salahudeen N, Ahmed AS, Al-Muhtaseb AH, Dauda M, Waziri SM, Jibril BY. Synthesis of gamma alumina from Kankara kaolin using a novel technique. Applied Clay Science, 2015; 105: 170-177.
[67] Dionigi C, Ivanovska T, Liscio F, Milita S, Corticelli F, Ruani G. Fabrication and properties of non-isolating γ-alumina mesofoam. Journal of Alloys and Compounds, 2016; 666: 101-107.
[68] Safaei M. Effect of temperature on the synthesis of active alumina by flash calcination of gibbsite. Journal of the Australian Ceramic Society, 2017; 53: 485-490.
[69] Saleh TA, Sulaiman KO, AL-Hammadi SA, Dafallaa H, Danmaliki GI. Adsorptive desulfurization of thiophene, benzothiophene and dibenzothiophene over activated carbon manganese oxide nanocomposite: with column system evaluation. Journal of cleaner production, 2017; 154: 401-412.
[70] Poyton AA, Varziri MS, McAuley KB, McLellan PJ, Ramsay JO. Parameter estimation in continuous-time dynamic models using principal differential analysis. Computers & chemical engineering, 2006; 30, 698-708.

To whom correspondence should be addressed: Aysar T. Jarullah, Chemical Engineering Department, College of Engineering, Tikrit University, Iraq; e-mail: A.T.Jarullah@tu.edu.iq